Constraints on neutron skin thickness and symmetry energy of ^{208}Pb through Skyrme forces and cluster model

M. Moghaddari Amiri[1)]   O. N. Ghodsi

Department of Physics, Faculty of Science, University of Mazandaran, P.O. Box 47415-416, Babolsar, Iran.

Abstract: We used the cluster structure properties of the ^{212}Po to estimate the neutron skin thickness of ^{208}Pb. For this purpose, we considered two important components: (a) alpha decay is a low energy phenomenon; therefore, one can expect that the mean-field, which can explain the ground state properties of ^{212}Po, does not change during the alpha decay process. (b) ^{212}Po has a high alpha cluster-like structure, two protons and two neutrons outside its core nucleus with a double magic closed-shell, and the cluster model is a powerful formalism for the estimation of alpha decay preformation factor of such nuclei. The slope of the symmetry energy of ^{208}Pb is estimated to be 75 ± 25 MeV within the selected same mean-fields and Skyrme forces, which can simultaneously satisfy the ground-state properties of parent and daughter nuclei, as their neutron skin thicknesses are consistent with experimental data.

1   Introduction

The α decay is among the most important decay modes for heavy and superheavy nuclei, and it has long been a useful tool in nuclear physics and astrophysics [1-6]. Measurements on α decays have long been employed for investigations on the nuclear structure [7-12]. Various theoretical models based on the shell model, fission-like model, and cluster model are applied in such studies [13-18].

During past decades, there has been an increasing desire to investigate the nuclear properties achieved by considering the influences of the neutron skin thickness (NST) on the alpha and cluster decay processes [19-22], where NST is defined by the difference between neutron and proton root mean square (RMS) radii, $\Delta r_{np} \equiv R_n - R_p$, and it can be related to the difference in nuclear asymmetric equation states inside and on the surface of the nucleus [23-25]. It is expected that heavy nuclei have a neutron skin structure, and that most of them are alpha emitters [26]. The NST consideration can impact the alpha core potential, reducing the calculated half-life against α decay [20, 22]. Microscopically, due to the ^{120}Sn (p, pα) ^{116}Cd, ^{12}C (^{6}Li, d) ^{16}O, and ^{16}O (^{6}Li, d) ^{20}Ni reactions, the α clustering on the nuclear surface and surface peak position of the wave function are investigated [27-29]. Furthermore, by investigating the absolute decay width within shell models, cluster-like shell models, and Bardeen-Cooper-Schrieffer approaches, the essential prerequisite for a realistic model of the mother nucleus indicated that it should correctly describe the cluster correlation in the surface region [1]. Therefore, studies on the surface of the nuclei, where the alpha cluster forms, have become critical.

Various studies have explored neutron and proton distributions and the measurement on RMS radii [19, 21, 23, 30, 31]. Although the RMS charge radii are accurately measurable by electron scattering, muonic atom X-rays, and the isotope shift [32], the neutron RMS radii of heavy nuclei are significantly less known. Furthermore, uncertainties of extracted neutron RMS radii are more than ten times larger than those of the charge radii [33]. Consequently, various theoretical and experimental studies have been employed for skin thickness of neutron and proton determinations [34-36]. Typically, the ^{208}Pb is a nucleus with the double magic closed-shell, with its NST being widely investigated for decades [23, 37]. Experimentally, the measured neutron skin thickness of ^{208}Pb ranges from 0.13 to 0.49 fm obtained by hadron scattering experiments involving pions, protons, and antiprotons, parity violation in electron scattering, measurements electric dipole polarizabilities of nuclei, and isospin diffusion in heavy-ion collisions [30, 33-37]. The

---

uncertainty may originate from limitations in the measurements.

Numerous approaches are employed to study the ground-state properties of nuclei, such as symmetry energies, binding energies, RMS radius, and nucleon density distributions. The Hartree-Fock model based on Skyrme forces is a successful approach for examining the ground-state properties of nuclei that includes several microscopic and phenomenological models, such as the relativistic Dirac-Brueckner-Hartree-Fock, nonrelativistic Brueckner-Hartree-Fock, and the nonrelativistic mean-field model based on Skyrme-like interactions [38-47]. Generally, the α decay process occurs at low energy levels, typically ($^{212}_{84}\text{Po} = {}^{208}_{82}\text{Pb} \otimes \alpha$), and this level of energy cannot cause sensible deviations in the ground-state and nuclear matter properties of an alpha emitter, suggesting that such investigations within the Hartree-Fock model and Skyrme forces are a good selection [48, 49]. Therefore, we carry out our studies by considering the same and constant mean-field, which simultaneously describing the ground-state properties of parent and daughter nuclei. In this work, by applying several Skyrme forces with their corresponding density distributions calculated from the Hartree-Fock model, we intend to examine the NST of the ^{208}Pb and properties of the α decay process for ^{212}Po.

This paper is organized as follows: the formalism of potential, half-life calculations, and the cluster formation model are illustrated in Sec. 2. Our results and discussion are presented in Sec. 3. The main results and conclusions are provided in Sec. 4.

2   Theoretical framework

2.1   Double-Folding formalism and α decay half-life

The total potential $V(r)$ is written by

$$V(r) = V_C(r) + V_N(r) + V_\ell(r), \quad (1)$$

where V_C, V_N, and V_ℓ are the Coulomb potential, nuclear potential, and centrifugal potential, respectively. In this study, we investigated the α decay of ^{212}Po that the transferred angular momentum for this decay process is zero. Therefore, the total potential is

$$V(r) = V_C(r) + \lambda V_F(r). \quad (2)$$

The nuclear part is obtained by the double-folding model within folding the densities of the α and the daughter nuclei with the effective M3Y interaction,

$$V_N = \lambda V_F(r) = \lambda \iint \rho_\alpha(r_\alpha) V_{\text{eff}} \rho_d(r_d) \mathrm{d}^3 r_\alpha \, \mathrm{d}^3 r_d, \quad (3)$$

where ρ_d and V_{eff} are the density of the daughter nucleus and the effective nucleon-nucleon interaction [50, 51], respectively. In this study, the ρ_d is calculated by Hartree-Fock formalism based on the Skyrme forces [38]. The density distribution function of the α particle, ρ_α, as used

in the folding calculations, has the Gaussian form [52]

$$\rho(r) = 0.4229 \, e^{-0.7024r^2}. \quad (4)$$

Here, we used the M3Y Reid-NN forces with a zero-range approximation for nucleon-nucleon interaction [53]. The parameter λ in Eq. (2) changes the folded potential strength that is known as the strength parameter that is determined using the Bohr-Sommerfeld quantization condition [54-56]:

$$\int_{r_1}^{r_2} \sqrt{\frac{2\mu}{\hbar^2}|V(r) - Q|} \, \mathrm{d}r = (2n+1)\frac{\pi}{2} = (G - \ell + 1)\frac{\pi}{2}, \quad (5)$$

where r_1, r_2 (and r_3 later) are classical turning points are obtained by $V(r) = Q$ (the α decay energy). The global quantum number G of a cluster state can be obtained by the Wildermuth condition [57]:

$$G = 2N + \ell = \sum_{i=1}^{4} g_i, \quad (6)$$

where N is the number of nodes of the α-core wave function; ℓ is the relative angular momentum of the cluster motion, and, g_i; is the oscillator quantum number of a cluster nucleon. For α decay, we can take G as

$$G = 2N + \ell = \begin{cases} 18, & N \leqslant 82, \\ 20, & 82 < N \leqslant 126, \\ 22. & N > 126. \end{cases} \quad (7)$$

The half-life of the α decay is $T_{1/2} = \hbar \ln 2 / \Gamma_\alpha$. In this relation, Γ_α is the α decay width of the cluster state within the Gurtviz and Kälbermann method, determined as [58]

$$\Gamma_\alpha = P_\alpha F \frac{\hbar^2}{4\mu} \exp\left(-2 \int_{r_2}^{r_3} k(r) \mathrm{d}r\right), \quad (8)$$

where F is normalization factor can be defined as below

$$F \int_{r_1}^{r_2} \frac{\mathrm{d}r}{k(r)} = 1, \quad (9)$$

and the wave number $k(r)$ is

$$k(r) = \sqrt{\frac{2\mu}{\hbar^2}|V(r) - Q|}. \quad (10)$$

Finally, P_α is the spectroscopic or preformation factor, calculated by $T_{1/2}^{\text{theo}}/T_{1/2}^{\text{exp}}$.

2.2   Cluster formation model

In the cluster formation model (CFM), it is assumed that the parent nucleus is a compilation of different cluster states [17]. For each preformation, there is a different wave function and a different Hamiltonian. Therefore, we assume that for each preformation or clusterization, there is a clusterization state represented by a wave function. If the parent nucleus has N different clusterization states with total energy E, the Hamiltonian H_i belongs to the ith clusterization defined with an ith wave function, therefore

$$H_i \Psi_i = E \Psi_i \qquad i = 1, 2, \ldots, N. \tag{11}$$

Therefore, this nucleus is described by a total time-independent wave function that is a linear combination of these clusterization orthonormalized wave functions

$$\Psi_i = \sum_{i=1}^{N} a_i \Psi_i, \tag{12}$$

where a_i are the amplitudes for the clusterization states of the complete set and within the orthogonality condition,

$$\sum_{i}^{N} |a_i|^2 = 1. \tag{13}$$

Each cluster has specific formation energy E_{fi} that

$$E_{fi} = |a_i|^2 E. \tag{14}$$

The probability of the α clusterization state P_α is equivalent to a_α^2. It can be calculated as:

$$P_\alpha = |a_\alpha|^2 = \frac{E_{f\alpha}}{E}. \tag{15}$$

Here, a_α and $E_{f\alpha}$ denote the coefficient of the α clusterization and the formation energy of an α cluster, respectively. E is composed of the $E_{f\alpha}$ and the interaction energy between α cluster and daughter nuclei. The detailed illustrations are provided in Ref. [17]. In the framework of CFM, the α cluster formation energy $E_{f\alpha}$ and total energy E of a considered system can be expressed as:

$$\begin{aligned} E_{f\alpha} =& 3B(A,Z) + B(A-4, Z-2) \\ & - 2B(A-1, Z-1) - 2B(A-1, Z), \end{aligned} \tag{16}$$

$$E = B(A,Z) - B(A-4, Z-2), \tag{17}$$

$B(A,Z)$ is the binding energy of the nucleus with mass number A and proton number Z. These defined energies in Eq. (16) and Eq. (17) belong to even-even nuclei, and for an odd atomic number or odd neutron number, the formation energies are calculated differently [59, 60].

Moreover, the formation probability of each cluster state calculates by the CFM can efficiently reproduce a more realistic formation probability, which follows the calculation of Varga et al. [13, 14].

3   Results and discussion

To investigate the NST of ^{208}Pb, we employed the density distributions that are self-consistently determined by Hartree-Fock calculations, based on different parameterizations of the Skyrme energy density functional. The Hamiltonian density functional used in this study and a more detailed discussion is presented in Ref. [61].

The energy per nucleon of an infinite asymmetric nuclear matter (ANM) with a proton fraction $\eta = Z/A$ in terms of the Skyrme energy density function is written as,

$$\begin{aligned} E_A =& \frac{3\hbar^2}{10m} k_F^2 H_{5/3} + \frac{t_0}{4} \rho \left[(x_0 + 2) - \left(x_0 + \frac{1}{2}\right) H_2 \right] \\ & + \frac{t_3 \rho^{\sigma+1}}{24} \left[(x_3 + 2) - \left(x_3 + \frac{1}{3}\right) H_2 \right] \\ & + \frac{3k_F^2}{40} \left\{ (2t_1 + 2t_2 + t_1 x_1 + t_2 x_2) \rho H_{5/3} \right. \\ & \left. + \left(\frac{t_2}{2} - \frac{t_1}{2} + t_2 x_2 - t_1 x_1 \right) \rho H_{8/3} \right\}, \end{aligned} \tag{18}$$

where $k_F = (3\pi^2 \rho/2)^{1/3}$ and $H_n(\eta) = 2^{n-1}[\eta^n + (1-\eta)^n]$. The parameters $x_0 - x_3$, $t_0 - t_3$, W_0, and σ are obtained by fitting different properties of nuclei, m is the nucleon mass, and $\rho = \rho_\pi + \rho_\nu$ is the nuclear density. The symmetry energy E_{sym} is defined by expanding Eq. (18) as a function of η and ρ that measures the isospin dependence of the nucleon-nucleon (NN) interaction as,

$$\begin{aligned} E_{\text{sym}}(\rho) =& \frac{1}{8} \left. \frac{\partial^2 E_A(\rho, \eta)}{\partial \eta^2} \right|_{\eta = \frac{1}{2}} = \frac{\hbar^2 k_F^2}{6m} \\ & - \frac{t_0}{4} \left(x_0 + \frac{1}{2}\right) \rho - \frac{t_3}{24} \left(x_3 + \frac{1}{2}\right) \rho^{\sigma+1} \\ & + \frac{k_F^2}{24} \{ (4t_2 - 3t_1 x_1 + 5t_2 x_2) \rho \}. \end{aligned} \tag{19}$$

The symmetry energy coefficient $a_{\text{sym}} = E_{\text{sym}}(\rho_0)$ is defined at the normal saturation density ρ_0. Further, another important quantity associated with the symmetry energy is the slope L of its density dependence. It can be written in the form

$$\begin{aligned} L =& 3\rho_0 \left. \frac{\partial E_{\text{sym}}(\rho)}{\partial \rho} \right|_{\rho_0} = \frac{\hbar^2 k_{F0}^2}{3m} \\ & - \frac{3t_0}{4} \left(x_0 + \frac{1}{2}\right) \rho_0 - \frac{t_3}{8} \left(x_3 + \frac{1}{2}\right) (\sigma + 1) \rho_0^{\sigma+1} \\ & + \frac{k_{F0}^2}{24} [5(4t_2 - 3t_1 x_1 + 5t_2 x_2) \rho], \end{aligned} \tag{20}$$

with $k_{F0} = (3\pi^2 \rho_0/2)^{1/3}$.

The volume incompressibility of ANM at saturation density is calculated as the derivative of pressure $P = \rho^2 \frac{\partial(E_A)}{\partial \rho}$ with respect to the number density ρ:

$$K = 9 \frac{\partial P}{\rho} = 9\rho^2 \left(\frac{\partial^2 E_A}{\partial \rho^2} \right). \tag{21}$$

To achieve an evaluation about the NST of nuclei, we calculated the neutron and proton RMS radii within nucleon density distributions, estimated by various Skyrme forces that they are expressed as

$$R_{n(p)}^{\text{rms}} = < R_{n(p)}^2 >^{1/2} = \left(\frac{\int r_{n(p)}^2 \rho_{n(p)}(r) \mathrm{d}r}{\int \rho_{n(p)}(r) \mathrm{d}r} \right)^{1/2}. \tag{22}$$

To calculate the NST value within RMS radii that are obtained by Eq. (22), we used the nucleon density distributions that are being estimated by the Hartree-Fock based

on the Skyrme forces. We assumed that the mean-fields and the Skyrme forces that describe the nuclear matter and ground-state properties of parent and daughter would not be affected by the α decay process, as the α decay process is a low energy phenomenon, and the amount of required energy for the transition from initial interior alpha clusterization state bound with daughter nucleus to free alpha particle and the daughter nucleus is not as significant, as it can actually cause a sensible variation in the ground-state properties of alpha emitters [17]. Therefore, from this viewpoint, we selected the same mean-field and Skyrme forces that can simultaneously describe the ground-state properties of ^{212}Po and ^{208}Pb.

We investigated the NST value of ^{208}Pb and its effects on the α decay process of ^{212}Po by employing various Skyrme NN interactions, associated with an extensive slope of the symmetry energy range from −49.7 to 100.1 MeV and with different nuclear matter incompressibility range from 200 MeV to 370 MeV, yielding different equations of state, binding energies, and RMS radii. The percentage of relative deviations for the calculated binding energies and the RMS radii for ^{212}Po and ^{208}Pb from their corresponding empirical values are presented in Fig. 1. The selected mutual forces SKxs25 ($L = 100.10$ MeV) [62], SGII ($L = 37.63$ MeV) [63], SKRA ($L = 53.04$ MeV) [64], Skm ($L = 49.34$ MeV) [65], KDE ($L = 41.42$ MeV) [66], SkS3 ($L = 51.74$ MeV) [67], SLy7 ($L = 46.94$ MeV) [68], SKSC3 ($L = 0.81$ MeV) [69], MSK3 ($L = 7.04$ MeV) [70], Gs ($L = 93.31$ MeV) [47], and Rs ($L = 86.39$ MeV) [47] are presented, which can simultaneously estimate the binding energies and RMS radii of parent and daughter nuclei with relative deviations of less than one percent. The experimental binding energies for ^{212}Po and its daughter ^{208}Pb are 1655.771 MeV and 1636.430 MeV, respectively. The experimental RMS radius of the daughter nucleus is 5.5012 fm [32]. Since the experimental RMS value for ^{212}Po has not been reported yet, the relation, $R_{ch}^{RMS} = (r_0 + r_1 A^{-2/3} + r_2 A^{-4/3}) A^{1/3}$ with $r_0 = 0.9071(13)$ fm, $r_1 = 1.105(25)$ fm, and $r_2 = -0.548(34)$ fm, is adopted for determining RMS radius ^{212}Po. This relation is obtained by fitting to the experimental data of the ground-state RMS radii for a wide range of the nuclei [32].

The calculated NST values of ^{208}Pb within Eq. (22) and the neutron and proton density distributions associated with the selected Skyrme forces as a function of the symmetry energy (L) are presented in Fig. 2. The results indicate an increasing trend for NST values as a function of the L. This tend could be owing to the density dependence of the nuclear symmetry energy. In principle, it can be obtained from the NST in heavy nuclei, since it is strongly correlated with the slope parameter L of the nuclear matter symmetry energy at saturation density [24, 71-74]. Hence, the Skyrme forces that have a different estimation regarding the nucleon distributions, yielding differ-
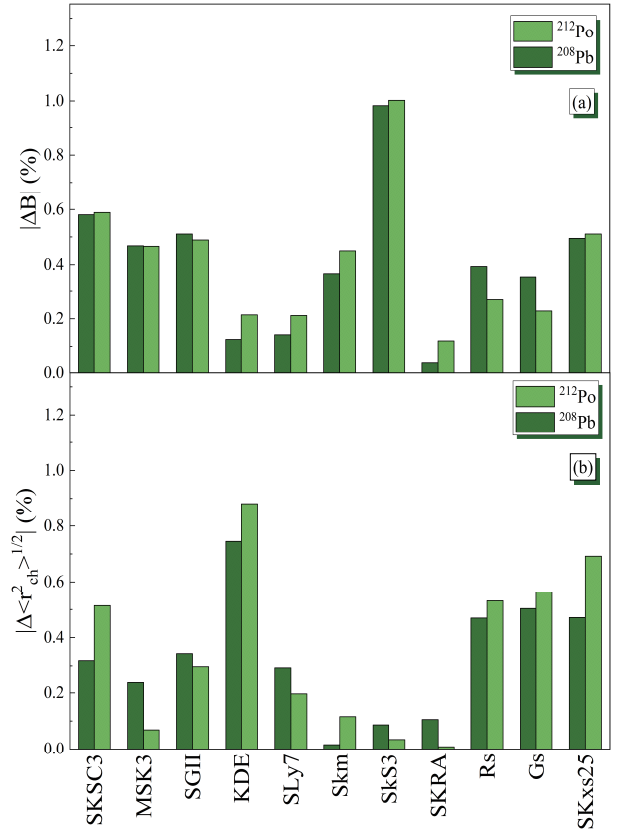

Fig. 1.   (color online) Percentage of relative deviations of theoretical binding energies and root-mean-square charge radii from their experimental data for ^{212}Po and ^{208}Pb nuclei in (a) and (b), respectively.

ent NST, it is possible that the NST to be affected by different symmetry energies corresponding to each Skyrme force. It can be expected that by increasing the nuclear symmetry energy, the differences between proton and neutron density distributions in the considered nucleus becomes more apparent [49, 75]. As shown in Fig. 2, the slope of the nuclear symmetry energy can be higher, where the neutron distribution is more different than the proton density distribution.

Since the neutron RMS radii of nuclei are less known in comparison with proton RMS radii, two extreme modes are usually employed to investigate the NST of the nuclei. The "neutron skin type" distribution is defined as $r_n > r_p$ and $a_n = a_p = 0.54$ fm and the "neutron halo type" distribution is understood as $r_n = r_p$ and $a_n > a_p$ [34]. Consequently, depending on which type is being considered for nuclei, the extracted NST contains uncertainty. Different experimental and theoretical investigations have been performed to evaluate NST to keep away from these extreme modes, especially for ^{208}Pb. For instance, the neutron skin thickness of ^{208}Pb was extracted as $\Delta R_{np} = 0.15 \pm 0.03$(stat.)$^{+0.01}_{-0.03}$(sys.) fm from coherent pion photo production cross-sections, and the lead radius
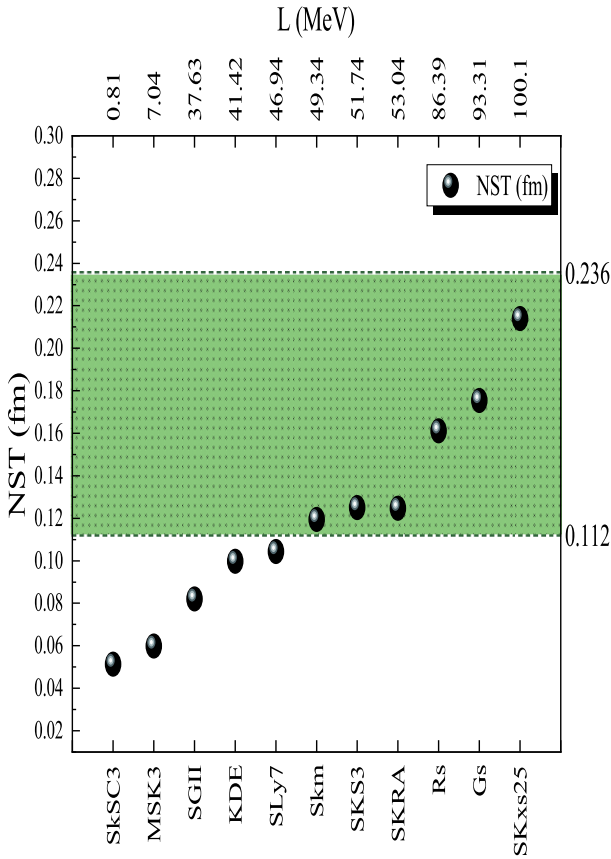
Fig. 2.   (color online) Calculated NST for selected Skyrme forces, colored region indicates NST values calculated by linear relationship presented in Ref. [34].
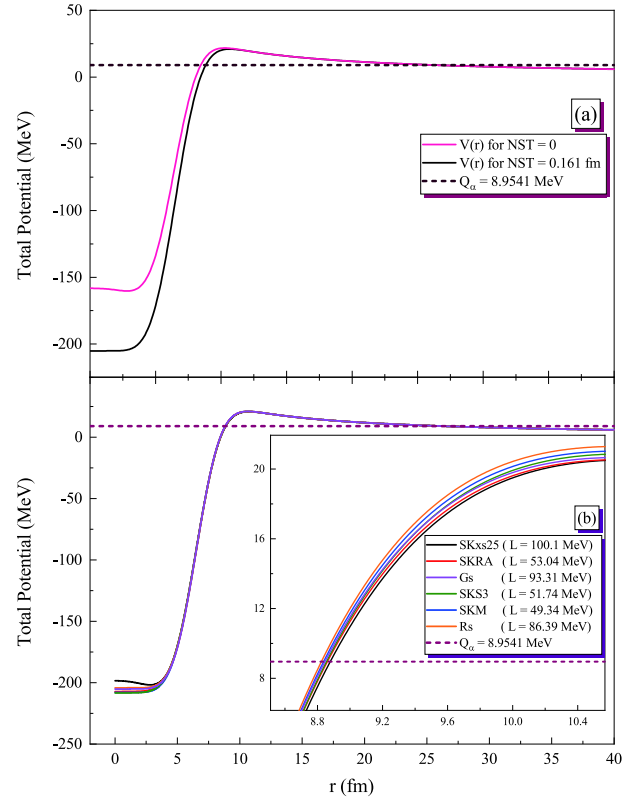

Fig. 3.   (color online) (a) Calculated total potential for $\Delta r_{np} = 0$ and $\Delta r_{np} = 0.161$ fm for Rs Skyrme force and (b) calculated total potential within different nucleon density distributions showing NST values in the range of the experimental data.

experiment (PREX) collaboration of JLab measured it as $\Delta R_{np} = 0.33^{+0.16}_{-0.18}$ fm through parity-violating electron scattering [76, 77]. Further, a linear relationship between ΔR_{np} with the isospin asymmetry $\delta = (N - Z)/A$ is found by antiprotonic atom X-ray data, which is expressed as [34]

$$\Delta R_{np} = (-0.04 \pm 0.03) + (1.01 \pm 0.15)\delta. \qquad (23)$$

This relationship yields a value of $\Delta R_{np} = 0.174(62)$ fm for ^{208}Pb, which is consistent with both the empirical values and theoretical predictions. The NST range of the ^{208}Pb extracted by this relationship is in the range from 0.112 to 0.236 fm, as indicated by the green band in Fig. 2. The Skyrme forces Skm, SKS3 , SKRA, Rs, Gs, and SKxs25 are located within this green band.

The effect of the NST consideration on the total potential calculation is shown in Fig. 3(a), typically for the Skyrme force Rs. The non-zero NST can cause a reduction in the total potential calculation. As illustrated in Fig. 2, the symmetry energy can affect the neutron skin thickness and nucleon density distributions. Hence, to investigate the effects of these nucleon density distributions that are theoretically suggested for ^{208}Pb on the total potential, we calculated the total potential by the double-

folding model and those neutron and proton density distributions that are corresponding to selected Skyrme forces. These influences on the calculated total potentials for sets of Skyrme forces SKxs25, SKRA, Skm, SkS3, Gs, and Rs that their NST values located in the range of experimental data, the green band in Fig. 2, are shown in Fig. 3(b), especially from the first turning point to the distance $r = 11$ fm. Differently calculated total potentials Fig. 3(b) represent that the choice of each characteristic nucleon density distribution can cause sensible variation in the calculation of the total potential.

By employing these total potentials, we calculated α decay half-lives and α formation probabilities that were obtained by $T^{theo}_{1/2}/T^{exp}_{1/2}$ presented in Fig. 4 and Fig. 5, respectively. To simultaneously satisfy the predictions of different theoretical models and experimental data, the evaluation of our estimated formation probabilities with the prediction of CFM would be beneficial, since the ^{212}Po has a high cluster-like structure.

The CFM illustrates each possible cluster formation probability in parent nuclei, such that its estimations will be more accurate for the nuclei with cluster-like structures, especially. This cluster-like structure supports the
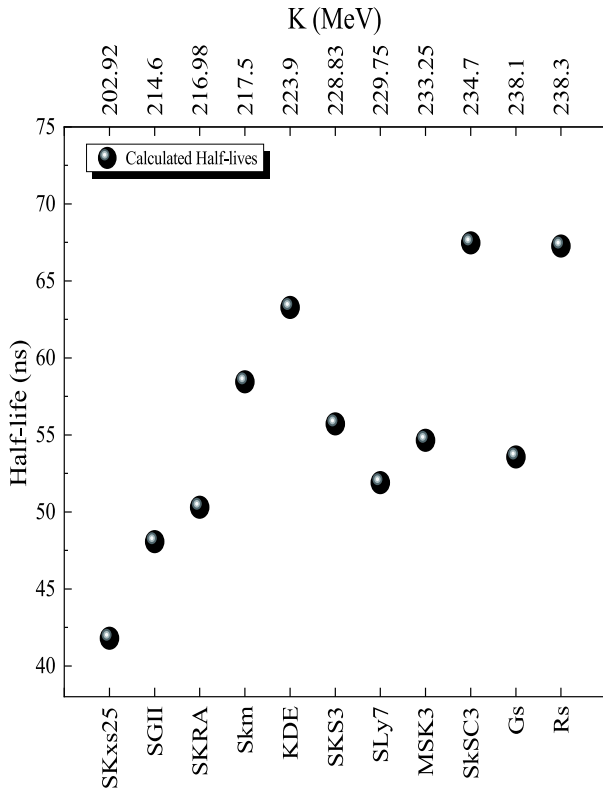
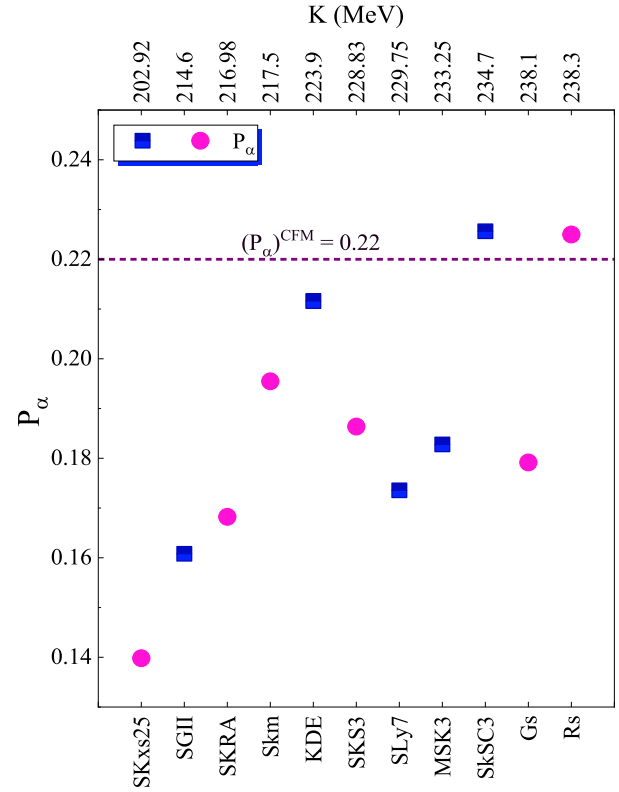Fig. 4.   Calculated α decay half-lives for each Skyrme force.

Fig. 5.   (color online) Calculated alpha formation probabilities for each Skyrme force. Dashed line depicts alpha formation probability within cluster model framework. Circles depict forces showing that their NST values are in the range predicted by Eq. (23) located within green band in Fig. 2.

alpha clustering occurrence at the surface of alpha emitters [1, 14, 57]. The estimated α cluster formation probability within CFM by the use of experimental binding energies in α decay for ^{212}Po is 0.22, indicated by the dashed line in Fig. 5. Further, from all Skyrme forces presented in Fig. 5, the estimated α formation probabilities of the SKxs25, SKRA, Skm, SkS3, Gs, and Rs indicate formation probabilities that correspond to the forces that their NST values satisfy in the experimental data. Therefore, the estimated α formation probabilities associated with these mentioned forces can be acceptable. The obtained results in Fig. 4 and Fig. 5 indicate that, although the α decay process is not capable of changing nuclear matter properties, different nucleon density distributions associated with the different symmetry energies can affect the α decay investigations, theoretically. The presented result in Fig. 4 indicates that the estimated half-lives within the SKxs25, SKRA, Skm, SkS3, Gs, and Rs Skyrme forces that their NST values are consistent with the experimental data, and they vary from 42 ns for SKxs25 (with $L = 100.1$ MeV) to 68 ns for Rs (with $L = 86.39$ MeV) following with the NST variation.

Moreover, from those estimated α formation probabilities within SKxs25, SKRA, Skm, SkS3, Gs, and Rs indicated by circular shapes in Fig. 5, the Skyrme force Rs can efficiently reproduce the formation probability calculated within CFM characterized by dashed line Fig. 5. Therefore, one can expect that Rs is one of the appropri-

ate forces for studying the nuclear properties of ^{208}Pb within α decay of ^{212}Po. The obtained results indicate that the α decay half-life and its preformation probability can be affected by 10% for ^{212}Po by assuming the α emitter in the different nuclear matter incompressibilities and symmetry energies. Such influences may imply that the theoretical studies for α decay can be affected by each nuclear matter property that is being considered for the nuclei in their ground-states. Although KDE and SKSC3 satisfy the alpha formation probability of the CFM, their NST values are not consistent with experimental data. Furthermore, the most common approaches are estimating the NST value of ^{208}Pb, which ranges from 0.14 to 0.18 fm [23, 34, 35, 63, 70, 78]. Our estimated NST value of ^{208}Pb is consistent with these measured values.

The values of the slope of the symmetry energy, L, corresponding to each Skyrme force, are shown in the upper axis of Fig. 2. The predicted values of NST increase with increasing L, and this increasing trend can be attributed to the variation of the symmetry energy. Because the symmetry energy correlates with the isospin asymmetry of the nuclei, one can expect that any variation in symmetry energy can cause variation in the nucleon density

distributions. Therefore, the higher symmetry energy can cause the differences between neutron and proton density distributions to become more apparent. As presented in Fig. 2, the slope of the symmetry energy for [208]Pb is estimated to be 75 ± 25 MeV, characterized by the sets of Skyrme forces SKxs25, SKRA, Skm, SkS3, Gs, and Rs, with their NST values located in the range of the experimental data. In contrast, due to the coherent pion photoproduction and PREX experiments on the measuring the NST value of the [208]Pb, and strong correlation between NST and the slope of the symmetry energy through the various cluster radio-activities, the estimated L values of the [208]Pb attributed to these experiments are $L(\rho_0) = 85 \pm 10$ MeV, and $L(\rho_0) = 80 - 170$ MeV, respectively [19]. Therefore, a good agreement can be seen between these reported values and our estimated slope of the symmetry energy for [208]Pb. However, the sets of Skyrme forces SKxs25, SKRA, Skm, SkS3, Gs, and Rs can theoretically be acceptable forces. According to the obtained results, the Rs force ($\Delta r_{np} = 0.161$ fm, $L = 86.39$ MeV, $K = 238.30$ MeV, and $a_{\text{sym}} = 29.20$ MeV can efficiently and simultaneously satisfy the experimental NST value, alpha formation probability estimates by CFM, and obtained slope of the symmetry energy for [208]Pb.

Typically, the half-height radius and diffuseness of proton density distribution, which are determined by fitted two-parameter Fermi distribution function to the density associated with Skyrme force Rs, are 6.5961 fm and 0.4865 fm, respectively, while these values for neutron density distribution are 6.8192 fm and 0.5496 fm, respectively. These estimated parameters indicate remarkable differences between half-height radii and diffuseness of proton and neutron density distributions, whereas they are not observed in the neutron skin type and neutron halo type. Thus, one can expect that some extreme states are being avoided by more detailed information on the nuclei properties.

4   Summary and conclusion

We investigated the NST value of [208]Pb and the nuclear properties of the α decay process for [212]Po. For evaluating the ground-state properties of [212]Po and [208]Pb, we used various Skyrme forces associated with an extensive slope of the symmetry energy. We conducted our investigations with the viewpoint that the employed mean-field and Skyrme forces remained constant throughout the α decay process of [212]Po. The influences of the selected neutron skin thickness on the α decay half-lives and formation probabilities are determined. To consider experimental NST values and CFM in our calculation, since the [212]Po has a high cluster-like structure, the Skyrme forces that could simultaneously reproduce the experimental NST values and cluster properties of the [212]Po were selected. The slope of the symmetry energy of the [208]Pb is estimated to be 75 ± 25 MeV by employing the sets of Skyrme forces SKxs25, SKRA, Skm, SkS3, Gs, and Rs, such that their NST values are consistent with the experimental data, where the Rs Skyrme force with an NST value 0.161 fm can efficiently satisfy the experimental and theoretical approaches. Furthermore, the estimated α formation probability by the Rs force corresponded to values calculated by the cluster model approach.

References

1   R. G. Lovas, R. J. Liotta, A. Insolia *et al.*, Phys. Rep., **294**: 265 (1998)
2   D. T. Akrawy and A. H. Ahmed, Phys. Rev. C, **100**: 044618 (2019)
3   J. H. Cheng, J. L. Chen *et al.*, Nucl. Phys. A, **987**: 350 (2019)
4   E. Olsen and W. Nazarewicz, Phys. Rev. C, **99**: 014317 (2019)
5   J. Dvorak *et al.*, Phys. Rev. Lett., **97**: 242501 (2006)
6   S. Peltonen, D. S. Delion, and J. Suhonen, Phys. Rev. C, **78**: 034608 (2008)
7   Z. G. Gan, J. S. Guo, X. L.Wu *et al.*, Eur. Phys. J. A, **20**: 385 (2004)
8   A. P. Leppänen *et al.*, Phys. Rev. C, **75**: 054307 (2007)
9   C. Xu and Z. Z. Ren, Phys. Rev. C, **74**: 014304 (2006)
10   F. P. Heßberger, S. Antalic, D. Ackermann *et al.*, Eur. Phys. J. A, **48**: 75 (2012)
11   A. Lopez-Martens *et al.*, Nucl. Phys. A, **852**: 15 (2011)
12   I. Ahmad, J. P. Greene, F. G. Kondev *et al.*, Phys. Rev. C, **87**: 054328 (2013)
13   K. Varga, R. G. Lovas, and R. J. Liotta, Phys. Rev. Lett., **69**: 37 (1992)
14   K. Varga, R. G. Lovas, and R. Liotta, Nucl. Phys. A, **550**: 421 (1992)

15   H. F. Zhang and G. Royer, Phys. Rev. C, **77**: 054318 (2008)
16   D. Ni and Z. Ren, Nucl. Phys. A, **828**: 348 (2009)
17   S. M. S. Ahmed, R. Yahaya, S. Radiman *et al.*, J. Phys. G, **40**: 065105 (2013)
18   D. Deng and Z. Ren, Phys. Rev. C, **93**: 044326 (2016)
19   C. Xu, Z. Ren, and J. Liu, Phys. Rev. C, **90**: 064310 (2014)
20   D. Ni and Z. Ren, Phys. Rev. C, **93**: 054318 (2016)
21   N. Wan, C. Xu, and Z. Ren, Nucl. Sci. Tech., **28**: 22 (2017)
22   M. Ismail and A. Adel, J. Phys. G: Nucl. Part. Phys., **44**: 125106 (2017)
23   D. Ni and Z. Ren, Phys. Rev. C, **92**: 054322 (2015)
24   A. E. L. Dieperink, Y. Dewulf *et al.*, Phys. Rev. C, **68**: 064307 (2003)
25   A. Krasznahorkay *et al.*, Nuclear Physics, A, **567**: 521 (1994)
26   C. Qi, Rev. Phys., **1**: 77 (2016)
27   K. Yoshida, K. Minomo, and K. Ogata, Phys. Rev. C, **94**: 044604 (2016)
28   T. Fukui, Y. Kanada-En'yo, K. Ogata *et al.*, Nucl. Phys. A, **983**: 38 (2019)
29   T. Fukui, Y. Taniguchi, T. Suhara *et al.*, Phys. Rev. C, **93**: 034606 (2016)
30   M. Warda, X. Vinas, X. Roca-Maza *et al.*, Phys. Rev. C, **80**: 024316 (2009)
31   M. Warda, M. Centelles, X. V. nas *et al.*, Acta Phys. Pol. B, **43**:

209 (2012)

32 I. Angeli and K. Marinova, At. Data Nucl. Data Tables, **99**: 69 (2013)

33 J. Zenihiro *et al*., Phys. Rev. C,82044611 (2010)

34 A. Trzcińska *et al*., Phys. Rev. Lett., **87**: 082501 (2001)

35 J. Jastrzębski, *et al*., Int. J. Mod. Phys. E, **13**: 343 (2004)

36 S. Wycech, F. J. Hartmann, J. Jastrzębski *et al*., Phys. Rev. C, **76**: 034316 (2007)

37 M. Centelles, X. Roca-Maza, X. Vinas *et al*., Phys. Rev. Lett., **102**: 122502 (2009)

38 D. Vautherin and D. M. Brink, Phys. Rev. C, **5**: 626 (1972)

39 B. G. Todd and J. Piekarewicz, Phys. Rev. C, **67**: 044317 (2003)

40 C. B. Das, S. Das Gupta, C. Gale *et al*., Phys. Rev. C, **67**: 034611 (2003)

41 B. Behera, T. R. Routray, A. Pradhan *et al*., Nucl. Phys. A, **753**: 367 (2005)

42 J. Rizzo, M. Colonna, and M. Di Toro, Phys. Rev. C, **72**: 064609 (2005)

43 E. van Dalen, C. Fuchs, and A. Faessler, Nucl. Phys. A, **741**: 227 (2004)

44 F. Sammarruca, W. Barredo, and P. Krastev, Phys. Rev. C, **71**: 064306 (2005)

45 J. Rong, Z. Y. Ma, and N. Van Giai, Phys. Rev. C, **73**: 014614 (2006)

46 W. Zuo, L. G. Cao, B. A. Li *et al*., Phys. Rev. C, **72**: 014005 (2005)

47 P. G. Reinhard, M. Rufa, J. Maruhn *et al*., Z. Phys. A, **323**: 13 (1986)

48 W. M. Seif, N. V. Antonenko, G. G. Adamian *et al*., Phys. Rev. C, **96**: 054328 (2017)

49 W. M. Seif and A. S. Hashem, Chin. Phys. C, **42**: 064104 (2018)

50 A. M. Kobos, B. A. Brown, R. Lindsay *et al*., Nucl. Phys. A, **425**: 205 (1984)

51 G. R. Satchler and W. G. Love, Phys. Rep., **55**: 183 (1979)

52 D. N. Basu, J. Phys. G, **29**: 2079 (2003)

53 D. T. Khoa and W. von Oertzen, Phys. Lett. B, **304**: 8 (1993)

54 B. Buck, A. C. Merchant, and S. M. Perez, At. Data Nucl. Data Tables, **51**: 559 (1995)

55 B. Buck, J. C. Johnston, A. C. Merchant *et al*., Phys. Rev. C, **53**: 2841 (1996)

56 B. Buck, A. C. Merchant, and S. M. Perez, At. Data Nucl. Data Tables, **54**: 53 (1993)

57 K. Wildermuth and Y. Tang, A Unified Theory of the Nucleus (Vieweg, Braunschweig, 1977)

58 S. A. Gurvitz and G. Kälbermann, Phys. Rev. Lett., **59**: 262 (1987)

59 D. Deng, Z. Ren, D. Ni *et al*., J. Phys. G, **42**: 075106 (2015)

60 J. G. Deng, J. C. Zhao, P. C. Chu *et al*., Phys. Rev. C, **97**: 044322 (2018)

61 M. Dutra, O. Lourenco, J. S. SaMartins *et al*., Phys. Rev. C, **85**: 035201 (2012)

62 B. A. Brown, G. Shen, G. C. Hillhouse *et al*., Phys. Rev. C, **76**: 034305 (2007)

63 N. Van Giai and H. Sagawa, Phys. Lett. B, **106**: 379 (1981)

64 M. Rashdan, Mod. Phys. Lett. A, **15**: 1287 (2000)

65 H. Krivine, J. Treiner, and O. Bohigas, Nucl. Phys. A, **336**: 155 (1980)

66 B. K. Agrawal, S. Shlomo, and V. K. Au, Phys. Rev. C, **72**: 014310 (2005)

67 J. M. G. Gómez, C. Prieto, and J. Navarro, Nucl. Phys. A, **549**: 125 (1992)

68 E. Chabanat, P. Bonche, P. Haensel *et al*., Nucl. Phys. A, **635**: 231 (1998)

69 J. M. Pearson, Y. Aboussir, A. K. Dutta *et al*., Nucl. Phys. A, **528**: 1 (1991)

70 F. Tondeur, S. Goriely, J. M. Pearson *et al*., Phys. Rev. C, **62**: 024308 (2000)

71 B. A. Brown, Phys. Rev. Lett., **85**: 5296 (2000)

72 C. J. Horowitz and J. Piekarewicz, Phys. Rev. Lett. **86**, 5647(2001); Phys. Rev. C **66**, 055803(2002)

73 R. J. Furnstahl, Nucl. Phys. A, **706**: 85 (2002)

74 S. Typel and B. A. Brown, Phys. Rev. C, **64**: 027302 (2001)

75 L. W. Chen, C. M. Ko, and B. A. Li, Phys. Rev. C, **72**: 064309 (2005)

76 C. M. Tarbert, D. P. Watts, D. I. Glazier *et al*.., Phys. Rev. Lett., **112**: 242502 (2014)

77 S. Abrahamyan, Z. Ahmed, H. Albataineh *et al*.., Phys. Rev. Lett., **108**: 112502 (2012)

78 J. M. Dong, L. J. Wang, W. Zuo *et al*., Phys. Rev. C., **97**: 034318 (2018)